

# Tracking control of variable stiffness hysteretic-systems using linear-parameter-varying gain-scheduled controller

D.T.R. Pasala<sup>1</sup>, S. Nagarajaiah\*<sup>2</sup> and K. M. Grigoriadis<sup>3</sup>

<sup>1</sup>Department of Civil and Environmental Engineering, Rice University, Houston, USA

<sup>2</sup>Department of Civil and Envi. Engrg. and Mechanical Engrg. and Mat. Sci., Rice University, Houston, USA

<sup>3</sup>Department of Mechanical Engineering, University of Houston, Houston, USA

(Received August 4, 2011, Revised March 18, 2012, Accepted March 20, 2012)

**Abstract.** Tracking control of systems with variable stiffness hysteresis using a gain-scheduled (GS) controller is developed in this paper. Variable stiffness hysteretic system is represented as quasi linear parameter dependent system with known bounds on parameters. Assuming that the parameters can be measured or estimated in real-time, a GS controller that ensures the performance and the stability of the closed-loop system over the entire range of parameter variation is designed. The proposed method is implemented on a spring-mass system which consists of a semi-active independently variable stiffness (SAIVS) device that exhibits hysteresis and precisely controllable stiffness change in real-time. The SAIVS system with variable stiffness hysteresis is represented as quasi linear parameter varying (LPV) system with two parameters: linear time-varying stiffness (parameter with slow variation rate) and stiffness of the friction-hysteresis (parameter with high variation rate). The proposed LPV-GS controller can accommodate both slow and fast varying parameter, which was not possible with the controllers proposed in the prior studies. Effectiveness of the proposed controller is demonstrated by comparing the results with a fixed robust  $\mathcal{H}_\infty$  controller that assumes the parameter variation as an uncertainty. Superior performance of the LPV-GS over the robust  $\mathcal{H}_\infty$  controller is demonstrated for varying stiffness hysteresis of SAIVS device and for different ranges of tracking displacements. The LPV-GS controller is capable of adapting to any parameter changes whereas the  $\mathcal{H}_\infty$  controller is effective only when the system parameters are in the vicinity of the nominal plant parameters for which the controller is designed. The robust  $\mathcal{H}_\infty$  controller becomes unstable under large parameter variations but the LPV-GS will ensure stability and guarantee the desired closed-loop performance.

**Keywords:** tracking control; quasi linear parameter varying system; linear parameter varying controller; gain-scheduled controller; robust  $\mathcal{H}_\infty$  controller; control of hysteretic systems

## 1. Introduction

Hysteresis is very common phenomenon observed in many electromechanical, structural and material systems at macro-, meso- micro- and nano-scales. Examples of such systems are gear systems, vibrating systems with umbilicals and smart materials like piezoceramic materials, magnetostrictive materials, electro-active polymers, electro-rheological and magneto-rheological fluids (Mehendale and Grigoriadis 2004, Song *et al.* 2007). Applications of these smart materials have been growing at a very fast rate in the last decade (Salapaka *et al.* 2002, Tan and Baras 2003, Song *et al.* 2005). However, the hysteresis behavior hinders the ability to exploit the unique properties possessed by these materials

---

\*Corresponding author, Professor, E-mail: [Satish.Nagarajaiah@rice.edu](mailto:Satish.Nagarajaiah@rice.edu)

such as the solid state actuation. This is due to the fact that the uncompensated hysteresis can cause a number of undesirable effects including poor performance, steady-state errors, limit cycle behavior and in some cases loss of stability (Oloomi and Shafai 2003, Mehendale *et al.* 2003, Pasala *et al.* 2009).

The most widely accepted approach for the control of hysteretic systems is by using inverse compensation in conjunction with a linear controller (Iyer and Tan 2009, Ganley *et al.* 2011). The basic idea of inverse compensation is to use the exact or approximate inverse hysteresis models to cancel the effects of the hysteresis nonlinearity (Smith 2001). The dynamics of the plant is represented as a linear term and nonlinear hysteretic term, the controller is designed for the linear part and the nonlinear term in the plant is canceled using the inverse mathematical model (Taware and Tao 2003, Krejci and Kuhnen 2001). Two well explored and tested examples of inverse compensation are piezoceramic sensors, actuators and magneto rheological dampers (Spencer and Nagarajaiah 2003, Liu 2008, Zapaterio *et al.* 2010, Mehendale 2005). Although the inverse compensation is simple and easy to implement it is effective only if the hysteretic system is either in the beginning or ending of a complex system. If the nonlinearity is sandwiched between two dynamic blocks then adaptive inversion methods have to be used (Taware and Tao 2003, Krejci and Kuhnen 2001). Even with these adaptive inversion schemes this approach suffers from few limitations: (1) the mathematical models assume that the systems with hysteresis have piecewise linear behavior, but this assumption is not true in case of many practical systems and (2) online adaptive inverse schemes are computationally intensive and also sensitive to experimental errors (Mehendale 2005).

A conservative way of compensating hysteresis is by linearizing the hysteresis curve over a range of displacements, resulting in a set of parameter (equivalent stiffness) values over which the robust stability and the performance must be achieved (Zhang *et al.* 2009). Then, a single robust linear time invariant controller can be designed to stabilize the system over a given range of parameter (equivalent stiffness) values. Tradeoff between the range of parameter variation and the tracking performance of the closed-loop system limits this approach (Pasala *et al.* 2008). A significantly less-conservative approach would be to design a time-varying controller expressed explicitly as a function of the system parameters, also called as gain-scheduled (GS) controller (Rugh and Shamma 2000). Formulation of the feedback control problem as a set of linear matrix inequalities is one significant leap to achieve this objective (Becker 1993, Wu *et al.* 1995, Apkarian and Adams 1998, Bai 2006). Due to the advent of powerful polynomial time computational algorithms, like the interior point algorithms, the computational time for calculating the controllers has decreased substantially (Skelton *et al.* 1998, Wu 1995, Zheng and Wu 2009).

The performance of the gain-scheduled controller depends on the assumed Lyapunov matrices. The Lyapunov matrices should be a function of parameter(s) to ensure the stability of the closed-loop system in the presence of parameter variations. The final controller calculated from the Lyapunov matrices will be a function of parameters and parameter-rates (time-derivative of the parameter). Note that the gain-scheduled controller has to be calculated, at every time-step, from the measured (or estimated) parameters and the parameter-rates. Since it may not be feasible to measure the parameter-rate in practical applications, the parameter-rate is replaced with the bounds of the corresponding parameter-rate. In summary, to design a gain-scheduled controller two elements are essential: (1) parameter dependent Lyapunov matrices and (2) the bounds on parameter-rates. If the Lyapunov matrices are constant then the designed controller is equivalent to the controller that can accommodate infinitely fast parameter-rates. This controller will be conservative in the sense that it is designed for a system that is assumed to be dependent on a parameter that changes infinitely fast.

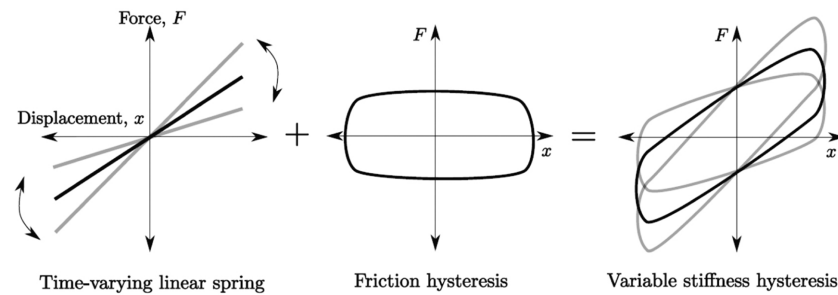


Fig. 1 Schematic diagram showing the variable stiffness hysteresis characteristics of SAIVS device [combination of linear time-varying spring and a friction hysteresis]

If the parameter dependency is incorporated in the Lyapunov matrices then the resulting controller will have a better performance on the system since it has taken into account the change in the parameter in real-time.

In this work, a systematic approach is developed to design a gain-scheduled controller for a specific class of smart systems called “variable stiffness hysteretic systems”. Variable stiffness hysteretic systems, shown in Fig. 1, comprise of a time-varying linear stiffness (slow-varying parameter) and stiffness of the friction-hysteresis (fast-varying parameter). Previously, Zhang (Zhang *et al.* 2009) have proposed an approach to design a gain-scheduled controller based on the tangential stiffness (scheduling parameter) for a vibration isolation system with hysteresis. The designed controller is based on constant Lyapunov function which means that the parameter-rate is arbitrarily fast. They assume that the bounds of parameters are known beforehand and design two fixed controllers for the plant at the minimum and maximum values of the parameter (tangential stiffness). Then the controller at every time-step is calculated by linearly interpolating between the controllers designed for the limiting parameter values. The controller proposed by Zhang *et al.* (2009) will not be effective for the systems with variable stiffness hysteresis properties. In Zhang *et al.* (2009) approach, a single parameter is used (sum of the slow-varying and fast-varying parameters) to design the gain scheduled controller. Since the fast-varying parameter has very high parameter-rate the effective rate of both the parameters combined will also have a very high parameter-rate. To overcome these limitations, in this study, both the parameters are considered separately and parameter dependent Lyapunov function is used in designing the gain-scheduled controller. Controller as an explicit function of the parameters is calculated from the parameter dependent Lyapunov matrices using projection method. Since the parameter-rate bounds have to be specified for both the parameters separately the designed GS controller will be able to accommodate the different rates of variation and will be sensitive to even the small variations of the slow-varying parameter. Since Zhang *et al.* (2009) used the total tangential stiffness of the variable hysteretic system as the parameter, different rates of slow- and fast-varying parameter cannot be incorporated in the controller design and hence they designed the controller using constant Lyapunov matrices.

The authors have also previously proposed the design of a gain scheduled controller for variable stiffness hysteretic systems scheduled based on two measured parameters (Pasala *et al.* 2009). In Pasala *et al.* (2009) although one of the parameters is slow-varying it is assumed that both the parameters are fast varying to simplify the controller design. In this work a new approach is proposed for the variable stiffness hysteretic systems taking into account the parameter-rates of the slow-varying-parameter and fast-varying-parameter separately. Both the parameters defined in this

paper can be calculated in real-time from the measured sensor output. The control objective in this study is to track a reference signal.

In this paper, the proposed gain-scheduled controller design is detailed with reference to the semi-active independently variable stiffness (SAIVS) system. Using the experimental data a nonlinear hysteretic model is developed for the SAIVS system (Bouc-Wen model). Bouc-Wen model, consisting of variable stiffness and hysteresis terms, is represented as a quasi linear parameter varying (LPV) system. The GS controller is constructed from the parameter dependent Lyapunov matrices, which are obtained as the optimal solution of the linear matrix inequalities (LMIs) that ensures the feasibility solution for the closed loop system performance. To demonstrate the effectiveness of proposed gain-scheduled controller the tracking response results are compared with a fixed robust  $\mathcal{H}_\infty$ -controller that is designed assuming the parameter variation as an uncertainty. The key contributions of this paper are (1) quasi-LPV formulation of the variable stiffness hysteretic systems and (2) decoupling the variable-stiffness into slow varying and fast varying parameters that allows incorporating the different parameter-rates in the controller design to achieve a better closed-loop performance.

The paper is organized as follows: Section-2 contains the description of the SAIVS system, experimental setup and analytical Bouc-Wen model for the SAIVS system. Section-3 consists of the new formulation showing the representation of Bouc-Wen model as a quasi-LPV system. Section-4 details the design of gain-scheduled controller using the LMI approach. Control objectives, constraints and closed-loop performance of the fixed robust  $\mathcal{H}_\infty$  controller and LPV-GS controller are also presented in section-4. Section-5 presents the tracking results from the numerical studies performed on the SAIVS system. Finally, some concluding remarks are presented in section-6.

## 2. SAIVS system

SAIVS system is a spring-mass system where the spring is replaced by SAIVS device (Mate 1998, Nagarajaiah and Mate 1998, Nagarajaiah and Sahasrabudhe 2006). Readers should pay attention to the two different terms used in this paper: SAIVS-device and the SAIVS-system. The SAIVS-device is a device which is equivalent to the parallel combination of a spring and a friction damper whereas the SAIVS-system is a series connection of SAIVS-device, mass and an actuator. Schematic diagram of the SAIVS system is shown in Fig. 2 and the experimental setup of the SAIVS system is shown in Fig. 3 (inset of Fig. 3 shows the schematic diagram of SAIVS-device). A rectangular steel frame is supported on four linear bearings and it is connected to the Modal-50 shaker (actuator) to actuate the frame along “X” direction. The ends of SAIVS device are connected to the frame (joint-2) and the servo-motor (joint-1) such that the stiffness of the SAIVS device can be

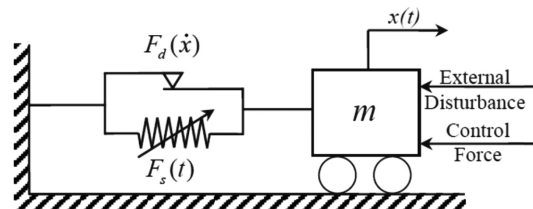


Fig. 2 Schematic diagram of the SAIVS system depicted as a combination of variable linear-stiffness element and nonlinear hysteresis element

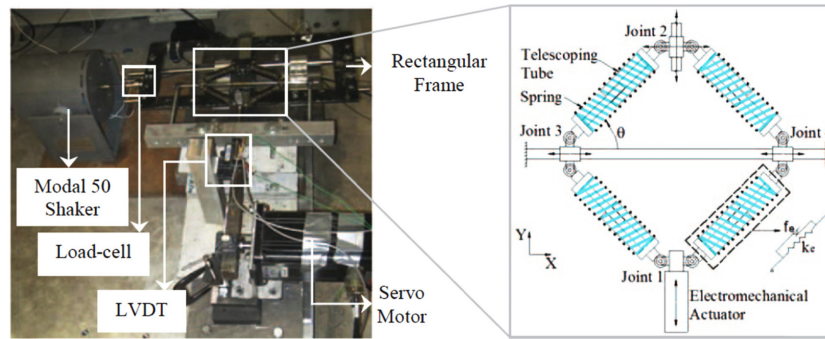


Fig. 3 Experimental setup of SAIVS system [Inset: Schematic diagram of the SAIVS device]

changed in real-time using the servo-motor; the connection is detailed in the later part of this section. The Modal-50 shaker is used as an actuator to exert the control force on the frame. Displacement of the frame along the “X”-direction is measured using a linear varying displacement transducer (LVDT). The dynamic equation of motion for the SAIVS system can be written as

$$m\ddot{x} + F_s(t) + F_d(\dot{x}) = F_{ctr}(t) + v(t) \quad (1)$$

where  $F_{ctr}(t)$  is the force exerted by Modal-50 shaker,  $v(t)$  is the external disturbance on the mass,  $m$  is total mass of rectangular frame.  $F_s$  is the force exerted due to the spring deformation and  $F_d$  is due to the friction in the elements. Total force  $F_s + F_d$  can be measured using the load-cell placed in series between the rectangular frame and the Modal-50 shaker, shown in Fig. 3.

## 2.1 SAIVS device

The SAIVS device was developed originally by Nagarajaiah and coworkers (Mate 1998, Nagarajaiah and Mate 1998, Nagarajaiah and Varadarajan 2005). Schematic of the SAIVS device is shown in the inset of Fig. 3. The SAIVS device can vary the stiffness continuously and smoothly. The device is controlled by an electric DC servo motor and a controller. The stiffness of the device is a function of its position. The SAIVS device consists of four springs arranged in a rhombus configuration as shown in Fig. 3. Each spring is located at an angle  $\theta$  to the guiding rail (rod that is passing through joint-3 and joint-4). Each of the four springs is supported on the inside by two telescoping tubes, which allow extension and compression of the springs and prevent them from buckling. As shown in Fig. 3, joint-1 is fixed in the “X”-direction and free to move in the “Y”-direction. Joint-1 is connected to a LVDT to measure the displacement,  $y_L(t)$ , in the “Y”-direction. Joint 2 is free to move in “X” and “Y” direction. Joints 3 and 4 can move in the “X”-direction only. At any instant the angle  $\theta$  can be calculated from the voltage reading in the LVDT using Eq. (2) (Mate 1998, Nagarajaiah and Mate 1998).

$$\theta(t) = \sin^{-1}\left(c_0 - \frac{y_L(t)}{L_s}\right) \quad (2)$$

where,  $y_L$  is the LVDT reading,  $c_0$  is a constant and  $L_s$  (4 in) is the length of each spring. Joint-2 is connected to the mass “ $m$ ”. Motion of joint-2 in the “X”-direction is governed by the Modal-50 shaker,

but in the “Y”-direction it is allowed to move freely. Force exerted by the SAIVS device on the mass is measured using the load-cell.

## 2.2 Analytical model for the SAIVS device

Four springs, shown in Fig. 3, of SAIVS are modeled as the stiffness elements. Each spring element in the device forms an angle  $\theta$  to the horizontal. This time varying angle  $\theta(t)$  is computed using the device position in the “Y”-direction, which can be calculated by measuring the displacement using the LVDT attached to joint-1. The device also possesses hysteretic damping because of the friction in the telescoping tubes and joints. For more elaborate study on the analytical modeling of the SAIVS device readers are referred to Nagarajaiah (Nagarajaiah and Varadarajan 2005). So, for any specific position, the restoring force,  $F_r$  (measured using the load-cell), in the SAIVS device can be written as

$$F_r(t, \dot{x}) = F_s(t) + F_d(\dot{x}, t) \quad (3)$$

where,  $F_s$  is the restoring force due to the deformation of linear spring,  $F_d$  due to the friction in the elements.  $x$ ,  $\dot{x}$  are the relative displacement and relative velocity, respectively, between joints 2 and 1 in the “X”-direction. The spring force,  $F_s$  at joint 2 in the “X”-direction is

$$F_s(t) = K_e \cos^2(\theta(t))x \quad (4)$$

where  $K_e$  is the stiffness of single spring. The force  $F_d$  is given by

$$F_d(\dot{x}, t) = \alpha_f' \cos(\theta(t))z(\dot{x}) \quad (5)$$

where  $\alpha_f'$  is a constant and  $z$  is the evolutionary variable (Sivaselvan and Reinhorn 2000, Wen 1976, Bouc 1967). The evolutionary variable (Bouc-Wen model) is dependent on the displacement and is given by

$$\frac{dz}{dx} = \left( \frac{1}{Y} - \frac{|z|^2}{Y} (\gamma \operatorname{sgn}(dx \cdot z) + \eta) \right) \quad (6)$$

For the SAIVS device developed,  $|F_d| < 0.25|F_s|$  and moreover the variation in  $\cos(\theta(t))$  is less than 10% about the mean value. So the Eq. (5) is further simplified by assuming,  $\alpha_f = \alpha_f' \cos(\theta_0)$  where,  $\theta_0$  is the mean value of  $\theta(t)$ . Consequently

$$F_d(\dot{x}) = \alpha_f z(\dot{x}) \quad (7)$$

This assumption is essential in order to represent the Bouc-Wen model as a simple LPV system from the implementation point of view (Apkarian and Adams 1998).

## 2.3 Experimental results

SAIVS system experimental setup is developed in the structural dynamics lab at Rice University. The measured mass,  $m$ , is 10 lbs, stiffness,  $K_e$  of each spring is 39 lb/in and the remaining parameters are estimated using an optimization algorithm.  $\alpha_f = 1.15$ ,  $\eta = 0.1$ ,  $\gamma = 0.9$  and  $Y = 0.02$  in. Comparison

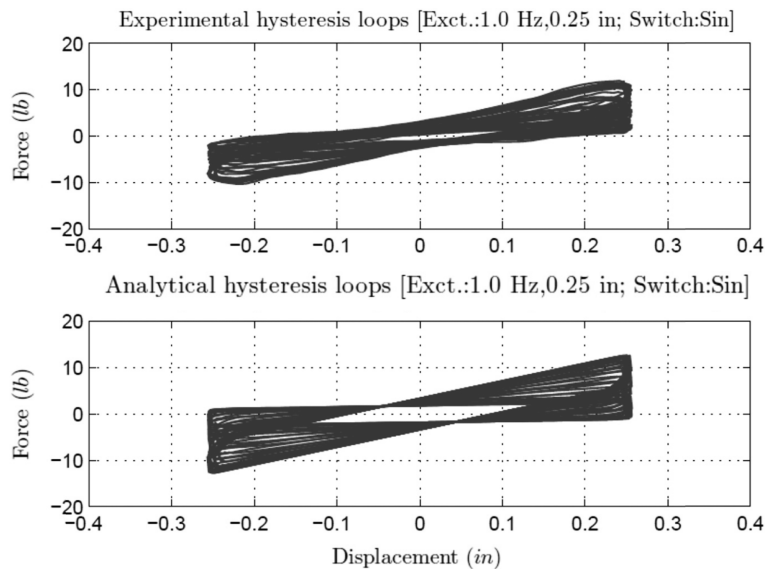


Fig. 4 Comparison of the experimental and analytical hysteresis loops of SAIVS system. Stiffness of the SAIVS device is changed using a sinusoidal wave of 0.325 Hz frequency

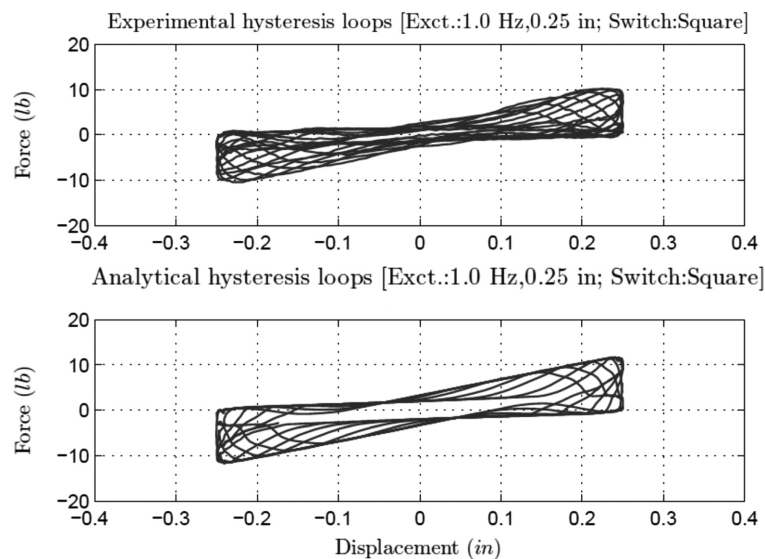


Fig. 5 Comparison of the experimental and analytical hysteresis loops of SAIVS system. Stiffness of the SAIVS device is changed using a square wave of 1 Hz frequency

of the analytical hysteresis loops and the experimental hysteresis loops shown in Figs. 4 and 5 indicate good agreement. A series of tests are performed to characterize the dynamic behavior of the device. Two signals are commanded from the data acquisition board: command signal to exert the external force on mass (excitation) and a command signal to change the stiffness of the SAIVS device (switching pattern). The system is subjected to harmonic excitation, using the Model-50 shaker, at an amplitude of 0.25 inches and frequency of 1 Hz in all the tests. Different switching patterns have

been tested experimentally for this harmonic excitation input. The experimental loops and the predicted analytical loops are shown in Figs. 4 and 5 for two switching patterns: low frequency sinusoidal switching and square switching respectively. Since the frequency of sinusoidal switching (0.325 Hz) is smaller compared to the excitation frequency (1 Hz), the stiffness variation is slow relative to the excitation and the hysteresis loops with different linear-stiffness can be seen in Fig. 4.

The hysteretic behavior due to the friction in the telescoping tubes and the other connections is evident in both the experimental force-displacement loops. In the experimental plots, the displacement (x-axis) data is measured using the LVDT and the force (y-axis) data is measured using the load-cell.

### 3. LPV formulation of the saivs system

Equation of motion given in Eq. (1) can be represented in state space form by assuming  $X_1 = x$  and  $X_2 = \dot{x}$  as the two states

$$\dot{X}_1 = X_2 \quad (8a)$$

$$\dot{X}_2 = -\frac{K_e \cos^2(\theta)}{m} X_1 - \frac{\alpha_f z}{m} + \frac{F_{ctr}}{m} \quad (8b)$$

Augmenting the system order by assuming  $X_3 = -\frac{\alpha_f}{m} z$  will result in a state space realization that is uncontrollable (Mehendale 2005).

So, assume the state variable  $X_3$  as shown in Eq. (9)

$$X_3 = -\frac{\alpha_f}{m} z + \frac{F_{ctr}}{m} \quad (9)$$

Now, Eq. (6) can also be written in the following form

$$\frac{dz}{dt} = \left( \frac{1}{Y} - \frac{|z|^2}{Y} \left( \gamma \operatorname{sgn} \left( \frac{dx}{dt} \cdot z \right) + \eta \right) \right) \frac{dx}{dt} \quad (10a)$$

$$\dot{z} = \left( \frac{1}{Y} - \frac{|z|^2}{Y} \left( \gamma \operatorname{sgn}(X_2 z) + \eta \right) \right) X_2 \quad (10b)$$

Differentiating Eq. (9) will result in Eq. (11)

$$\dot{X}_3 = -\frac{\alpha_f}{m} \dot{z} + \frac{\dot{F}_{ctr}}{m} \quad (11)$$

Replacing  $\dot{z}$  in Eq. (11) with Eq. (10b) will result in

$$\dot{X}_3 = -\frac{\alpha_f}{m} \left( \frac{1}{Y} - \frac{|z|^2}{Y} \left( \gamma \operatorname{sgn}(\dot{x} z) + \eta \right) \right) X_2 + \frac{\dot{F}_{ctr}}{m} \quad (12)$$

The state space representation of the approximated SAIVS system as a controllable quasi-LPV system is shown below

$$\begin{bmatrix} \dot{X}_1 \\ \dot{X}_2 \\ \dot{X}_3 \end{bmatrix} = \begin{bmatrix} 0 & 1 & 0 \\ -\frac{K_e \rho_1}{m} & 0 & 1 \\ 0 & -\frac{\alpha_f \rho_2}{m Y} & 0 \end{bmatrix} \times \begin{bmatrix} X_1 \\ X_2 \\ X_3 \end{bmatrix} + \begin{bmatrix} 0 \\ 0 \\ \frac{1}{m} \end{bmatrix} \times \dot{F}_{ctr} \quad (13)$$

$$y = [1 \ 0 \ 0] \times [X_1 \ X_2 \ X_3]^T \quad (14)$$

where

$$\rho_1 = \cos^2(\theta) \quad (15)$$

$$\rho_2 = (1 - \gamma \operatorname{sgn}(X_2)z|z| - \eta z^2) \quad (16)$$

Since the parameter  $\rho_2$  is state dependent the representation in Eq. (13) is called the quasi-LPV system. The designed controller is scheduled based on the parameters  $\rho_1$  and  $\rho_2$ . Parameter  $\rho_1$  is representative of the linear time-varying stiffness of the spring. Parameter  $\rho_2$  is proportional to the instantaneous stiffness of the friction assembly (compare Eqs. (6) and (16)). At any instant,  $\rho_1(t)$  is calculated from  $y_L(t)$  using Eqs. (2) and (15).  $\rho_2$  is calculated from the load-cell data,  $F_r$ , in the following steps:

- Since  $\theta(t)$  is known,  $F_s(t)$  is calculated using Eq. (4)
- $F_d$  is calculated from  $F_r$  and  $F_s(t)$  using Eq. (3)
- The change of  $F_d$  with respect to  $x$  is calculated  $\left(\frac{dF_d}{dx}\right)$
- From Eq. (7),  $\frac{dF_d}{dx} = \alpha_f \frac{dz}{dx}$ ,  $\frac{dz}{dx}$  is calculated
- $\rho_2$  is obtained from  $\frac{dz}{dx}$  by multiplying with  $Y$

It should be noted that the control force on the right hand side of Eq. (13) has a time derivative. Gain scheduled controller is designed for system in Eq. (13) so, when the controller is implemented experimentally an integration-operator,  $1/s$ , has to be added to the plant and the equivalent closed loop system can be visualized as the one shown in Fig. 6.

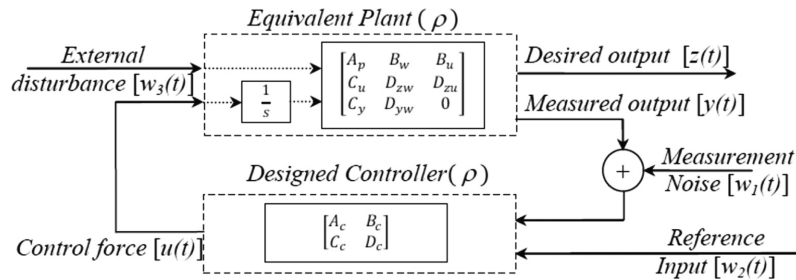


Fig. 6 Equivalent closed loop system

#### 4. Controller design

Designing a gain scheduled controller for a generalized LPV plant is detailed in this section. It is assumed that the parameter and the parameter-rate are bounded and are known beforehand. Consider a generalized LPV plant

$$\dot{X} = A_p(\rho)X + B_w(\rho)w + B_u(\rho)u \quad (17)$$

$$z = C_z(\rho)X + D_{zq}(\rho)w + D_{zu}(\rho)u \quad (18)$$

$$y = C_y(\rho)X + D_{yw}(\rho)w \quad (19)$$

where,  $X$  is the internal states of the plant,  $w$  is the external disturbance,  $u$  is the control force,  $z$  is the desired output and  $y$  is the measured output shown in Fig. 6.  $A_p \in \mathbb{R}^{n_s \times n_s}$ ,  $B_w \in \mathbb{R}^{n_s \times n_d}$ ,  $B_u \in \mathbb{R}^{n_s \times n_u}$ ,  $C_z \in \mathbb{R}^{n_e \times n_s}$ ,  $D_{zw} \in \mathbb{R}^{n_e \times n_d}$ ,  $D_{zu} \in \mathbb{R}^{n_e \times n_u}$ ,  $C_y \in \mathbb{R}^{n_y \times n_s}$  and  $D_{yw} \in \mathbb{R}^{n_y \times n_d}$  and the time varying parameter  $\rho := (\rho_1 \ \rho_2)$ .  $n_s$  is the number of states,  $n_d$  is the number of exogenous inputs,  $n_u$  is the number of outputs from the controller (Control force),  $n_e$  is the number of desired outputs,  $n_y$  is the number of measured outputs fed to the controller. Full order LPV gain-scheduled output-feedback controller is assumed to be of the form

$$\dot{X}_c = A_c(\rho, \dot{\rho})X_c + B_c(\rho, \dot{\rho})y \quad (20)$$

$$u = C_c(\rho, \dot{\rho})X_c + D_c(\rho, \dot{\rho})y \quad (21)$$

where,  $X_c$  is the states of the controller,  $A_c \in \mathbb{R}^{n_s \times n_s}$ ,  $B_c \in \mathbb{R}^{n_s \times n_y}$ ,  $C_c \in \mathbb{R}^{n_u \times n_s}$  and  $D_c \in \mathbb{R}^{n_u \times n_y}$ . The following theorem states the conditions for the existence of the controller that stabilizes the closed loop system and ensures the desired performance.

**Theorem:** Controller,  $\begin{bmatrix} A_c & B_c \\ C_c & D_c \end{bmatrix}$ , that satisfies the closed-loop  $\mathcal{L}_2$  bound,  $\frac{\int_0^t z^T z d\tau}{\int_0^t w^T w d\tau} \leq \gamma^2$ ,  $\forall t \geq 0$  exist

if there exists parameter dependent Lyapunov matrices  $P(\rho)$  and  $Q(\rho)$  such that for all the pairs of  $(\rho, \dot{\rho})$  satisfy the following infinite-dimensional linear matrix inequalities (Apkarian and Adams 1998)

$$\begin{bmatrix} \mathcal{N}_{P_1}^T & \mathcal{N}_{P_2}^T & 0 \\ 0 & 0 & I \end{bmatrix} \begin{bmatrix} \hat{P} & PB_w & C_z^T \\ B_w^T P & -\gamma I & D_{zw}^T \\ C_z & D_{zw} & -\gamma I \end{bmatrix} \begin{bmatrix} \mathcal{N}_{P_1} & 0 \\ \mathcal{N}_{P_2} & 0 \\ 0 & I \end{bmatrix} < 0 \quad (22)$$

$$\begin{bmatrix} \mathcal{N}_{Q_1}^T & \mathcal{N}_{Q_2}^T & 0 \\ 0 & 0 & I \end{bmatrix} \begin{bmatrix} \hat{Q} & QC_z^T & B_w \\ C_z Q & -\gamma I & D_{zw} \\ B_w^T & D_{zw}^T & -\gamma I \end{bmatrix} \begin{bmatrix} \mathcal{N}_{Q_1} & 0 \\ \mathcal{N}_{Q_2} & 0 \\ 0 & I \end{bmatrix} < 0 \quad (23)$$

$$\begin{bmatrix} P & I \\ I & Q \end{bmatrix} > 0 \quad (24)$$

where,  $\hat{P} = \dot{P} + PA_p + A_p^T P, \hat{Q} = -\dot{Q} + QA_p^T + A_p Q, [\mathcal{N}_{P_1} \mathcal{N}_{P_2}]^T \in null([C_y \ D_{yw}])$  and  $[\mathcal{N}_{Q_1} \mathcal{N}_{Q_2}]^T \in null([B_y^T \ D_{zu}^T])$ .

The controller can be constructed from the Lyapunov matrices  $P(\rho)$  and  $Q(\rho)$  using the projections method (explained in section 4.1). Parameter dependent Lyapunov matrices are generally of the form  $P(\rho) = P_0 + P_1\rho + \dots + P_i\rho^i, Q(\rho) = Q_0 + Q_1\rho + \dots + Q_j\rho^j$ , where,  $P_0, P_1, \dots, P_i$  and  $Q_0, Q_1, \dots, Q_j$  are constant matrices.

In the above theorem, there are two unknowns (in Eqs. (22)-(24)), the parameter dependent Lyapunov matrices ( $P(\rho)$  and  $Q(\rho)$ ) and the closed loop  $\mathcal{L}_2$  norm,  $\gamma$ . If minimum norm,  $\gamma$ , of the system is known then any pair of Lyapunov matrices,  $P(\rho)$  and  $Q(\rho)$ , that satisfy Eqs. (22)-(24) can be calculated. Likewise, if the Lyapunov matrices,  $P(\rho)$  and  $Q(\rho)$ , are known then the minimum achievable  $\mathcal{L}_2$  norm of the system can be calculated.

Since Eqs. (22)-(24) are a set of linear matrix inequalities, calculating the parameter dependent Lyapunov matrices ( $P(\rho)$  and  $Q(\rho)$ ) can be stated as a convex optimization problem. The objective is to find the minimum  $\gamma$  for all the possible values of  $P(\rho)$  and  $Q(\rho)$ , subject to the inequality constraints mentioned in Eqs. (22)-(24). Note that the optimization should hold true for all the pairs of  $(\rho, \dot{\rho})$ . Essentially, the inequality constraints have to be evaluated at every parameter value within the known bound of parameters and this will be an infinite dimensional problem.

Solving the infinite dimensional problem is the price paid for allowing the parameter dependency into the Lyapunov matrices. This infinite-dimensional problem is reduced to a finite dimensional problem by gridding the parameter space and ensuring that Eq. (22-24) are valid at all the grid points.

#### 4.1 Controller construction using projections method

The controller matrices can be calculated based on the obtained parameter dependent Lyapunov matrices ( $P(\rho)$  and  $Q(\rho)$ ) using the following projections method (Apkarian and Adams, 1998).  $D_{zu}$  and  $D_{yw}$  have to be full-column and full-row rank respectively to apply this method. First step is to calculate the matrix  $D_c$  such that

$$\sigma_{\max}(D_{zw} + D_{zu}D_cD_{yw}) < \gamma \tag{25}$$

where  $\sigma_{\max}$  is the spectral norm (the spectral norm of a matrix  $M$  is the largest singular value of  $M$ ). Then, calculate  $D_{cl}, \hat{B}_c, \hat{C}_c$  and  $\hat{A}_c$  using the following equations

$$D_{cl} = D_{zw} + D_{zu}D_cD_{yw} \tag{26}$$

$$\begin{bmatrix} 0 & D_{yw} & 0 \\ D_{yw}^T & -\gamma I & D_{cl}^T \\ 0 & D_{cl} & -\gamma I \end{bmatrix} \begin{bmatrix} \hat{B}_c^T \\ \hat{a} \end{bmatrix} = - \begin{bmatrix} C_y \\ B_w^T P \\ C_z + D_{zu}D_cC_y \end{bmatrix} \tag{27}$$

$$\begin{bmatrix} 0 & D_{zu}^T & 0 \\ D_{zu}^T & -\gamma I & D_{cl} \\ 0 & D_{cl}^T & -\gamma I \end{bmatrix} \begin{bmatrix} \hat{C}_c \\ \hat{a} \end{bmatrix} = - \begin{bmatrix} B_u^T \\ C_z Q \\ (B_w + B_uD_cD_{yw})^T \end{bmatrix} \tag{28}$$

$$\hat{A}_c = -(A_p + B_u D_c C_y) + \left[ PB_w + \hat{B}_c D_{yw} \quad (C_z + D_{zu} D_c C_u)^T \right] \begin{bmatrix} -\gamma I & D_{cl}^T \\ D_{cl} & -\gamma I \end{bmatrix}^{-1} \begin{bmatrix} (B_w + B_u D_c D_{yw})^T \\ C_z Q + D_{zu} \hat{C}_c \end{bmatrix} \quad (29)$$

Using the variables calculated from Eqs. (26)-(29), the controller state space matrices  $A_c$ ,  $B_c$  and  $C_c$  can be calculated using the following equations

$$A_c = N^{-1}(\hat{A}_c - P(A_p - B_u C_c C_y) - \hat{B}_c C_y Q - P B_u C_c) M^T \quad (30)$$

$$B_c = N^{-1}(\hat{B}_c - P B_u D_c) \quad (31)$$

$$C_c = (\hat{C}_c + D_c C_y Q) M^T \quad (32)$$

where,  $N$  and  $M$  are calculated based on the guidelines suggested by Apkarian and Adams (Apkarian and Adams 1998) from the practical point of view. Assuming  $P = P(\rho)$  and  $Q = Q_0$  where  $Q_0$  is constant (independent of parameter).  $N$  and  $M$  can be obtained from  $P$  and  $Q$  using the following selection,  $N := I - P(\rho)Q_0$  and  $M := I$ . Parameter dependent Lyapunov matrices assumed in this paper are of the following form

$$P(\rho) = P_0 + P_1 \rho_1 + P_2 \rho_2 \quad (33)$$

$$Q(\rho) = Q_0 \quad (34)$$

where,  $P_0, P_1, P_2$  are  $Q_0$  are constant matrices that ensure the stability of the closed-loop system and also result in optimal norm of the closed-loop system. These matrices are the optimization variables in minimizing the closed-loop norm of the system and Eqs. (22)-(24) are the inequality constraints.

#### 4.2 Control objectives and constraints

The main objective of the designed closed loop system is to track the commanded input. Numerically, the performance objective is specified in terms of the ratio of induced  $\mathcal{L}_2$  norm. Optimal controller is obtained by minimizing the energy-to-energy norm from the disturbance signal to the error signal. Additional specifications include:

**(a) Control constraint:** Assuming there is actuator saturation, control effort exerted should be limited and should not exceed a predefined value. In this case  $|F_{ctr}| < 4lb$

**(b) Performance objectives:** Settling and overshoot have to be minimized. This is governed by the choice of frequency dependent weighting functions or penalty functions.

**(c) Noise rejection:** Impact of the measurement noise on the desired objective has to be minimized.

**(d) Robustness specifications:** Stability and the tracking performance of the closed-loop system has to be ensured for different switching cases of the SAIVS

To find the optimal controller,  $\mathcal{H}_\infty$ -norm of the closed-loop system, specified as a ratio of induced  $\mathcal{L}_2$  norms of weighted desired-outputs to the exogenous inputs, has to be minimized (Wu 1995 Wu *et al.* 1997). To design a fixed and robust  $\mathcal{H}_\infty$  controller, only the nominal plant is used (Doyle *et al.* 1989). Robust- $\mathcal{H}_\infty$  controller will be referred as just  $\mathcal{H}_\infty$  controller from hereon. LPV gain scheduled controller is calculated for the SAIVS system using the approach proposed by Apkarian and Adams (Apkarian and Adams 1998). First, parameter dependent Lyapunov matrices that minimize the  $\mathcal{H}_\infty$ -norm of the closed loop systems are calculated and then the state space matrices of the controller

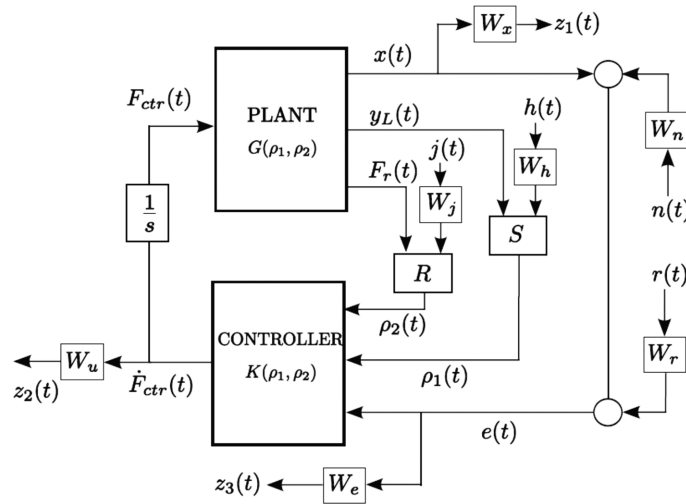


Fig. 7 Augmented closed loop block diagram with detailed interconnections for LPV-GS Controller

are calculated using Eqs. (30)-(32).

Block diagram of the closed-loop LPV-GS controller with all the interconnections is shown in Fig. 7. To design the LPV-GS plant state space equations have to be augmented by incorporating the other exogenous inputs, measurement noise  $n(t)$ ,  $h(t)$  and  $j(t)$  and reference signal  $r(t)$ , and the frequency dependent weights,  $W_e$ ,  $W_u$ ,  $W_j$ ,  $W_h$ ,  $W_n$ ,  $W_r$  and  $W_x$ , as shown in Fig. 7. For the analytical model calculated in the previous section, fixed robust  $\mathcal{H}_\infty$  controller is designed by choosing the nominal values for the parameters  $\rho_1$  and  $\rho_2$  and the parameter variation is represented as an uncertainty.

$r(t)$  is the reference displacement to be tracked.  $n(t)$ ,  $h(t)$  and  $j(t)$  are the experimental noise signals in measuring  $x$ ,  $y_L$  and  $F_d$  respectively.  $W_n(s)$  is the weight function for the measurement noise of  $x$ ,  $W_h(s)$  is the weight function for the measurement noise of  $y_L$ ,  $W_j(s)$  is the weight function for the measurement noise of  $F_d$ ,  $W_r(s)$  is the weight function for the reference input,  $W_u(s)$  is the weight function for the control input,  $W_e(s)$  is the weight function for the tracking error and  $W_x(s)$  is the weight function for the plant output.  $z_1 = W_x x$  is the weighted output,  $z_3 = W_e e$  is the weighted error signal and  $z_2 = W_u F_{ctr}$  is the weighted control force.  $S$  and  $R$  in Fig. 7 represents the blocks to calculate the parameters  $\rho_1$  (using Eqs. (2) and (15)) and  $\rho_2$  (using Eqs. (10(b)) and (16)) from the measured experimental data. The exogenous inputs acting on the system are  $[r(t), n(t), h(t), j(t)]^T$  and the desired outputs to be minimized are  $[z_1(t), z_2(t), z_3(t)]^T$ . The frequency dependent weights are chosen to reflect the performance objectives and the control constraints (Apkarian and Gahinet, 1995, Skogestad and Postlethwaite 1996).

For example,  $W_e$  (weight function for the tracking error signal), should have a high magnitude at low frequencies because the tracking performance of the closed-loop system should be effective at low frequencies. At high frequencies, to reject the measurement noise, the magnitude of  $W_e$  should be very low. In other words, the error signal should be multiplied with a large value at low frequencies for the controller to respond quickly but at high frequencies the error is scaled down or penalized so that the controller will not respond to the high frequency signal, which is generally measurement noise. Ideally,  $W_e$  should have a pure integrator in it, but to avoid the computational problems in finding the controller in MATLAB (Apkarian *et al.* 1995)  $W_e/1/(s+0.0001)$  is chosen.

We suggest the readers to the book by Skogestad and Postlethwaite (1996) for detailed procedure on weight function selection.

The Bouc-wen model, representing the friction, in Eq. (6), is highly nonlinear and represents a stiff-differential equation. For this reason the closed-loop response of the hysteretic system is calculated using adaptive, variable time-step solvers. Since these solvers are not supported in the data-acquisition system used in the experimental setup, described in section 2.3, the developed controller could not be implemented experimentally. Only the numerical results are presented from hereon.

#### 4.3 Closed-loop performance

To show the effectiveness of the LPV GS controller, bode plots of the closed-loop transfer function (for a set of frozen parameter values) from the reference-signal to the output  $x(t)$  for a closed loop system with fixed robust  $\mathcal{H}_\infty$  controller (designed for nominal plant) and a LPV-GS controller at various parameter grid points are shown in Fig. 8 and Fig. 9 respectively.  $\rho_1$  has grid points at [0.15 0.3 0.45 0.6] and  $\rho_2$  has grid points at [0.1 0.5 0.9 1.3 1.7]. Ideal Bode plot for the tracking control should have a flat end at 0 dB for the low frequencies and should roll off with a steep slope at high frequencies to have good noise rejection attributes. The frequency dependent weights are chosen in such a way that this objective is achieved.

Results shown in Figs. 8 and 9 are for a set of frozen parameter values. These plots do not depict the behavior of the system for time-varying parameters. From the plots shown in Fig. 8 it can be seen that the fixed- $\mathcal{H}_\infty$  controller is effective only when the uncertain plant parameters are close to the nominal plant parameters. Magnitude of the closed-loop system with  $\mathcal{H}_\infty$  controller varies from -50 dB to 25 dB and the phase fluctuates between -180° and 180° for frequencies less than 10 rad/sec. Where as in the case of LPV-GS controller, shown in Fig. 9, the performance of the closed-loop system is very consistent and the Bode plots for all the sets of parameters have a flat end till 20 rad/sec frequency. This shows the effectiveness of the gain-scheduled controller.

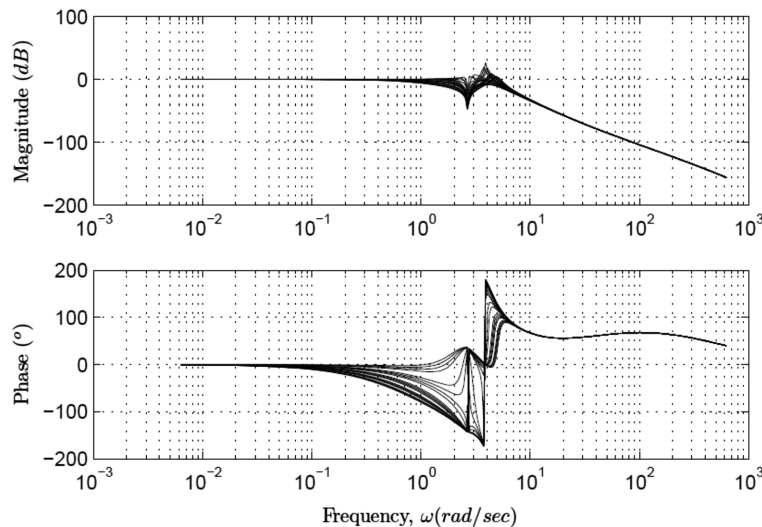


Fig. 8 Frozen parameter bode plots of  $\mathcal{H}_\infty$ -controller: Transfer function from reference to output

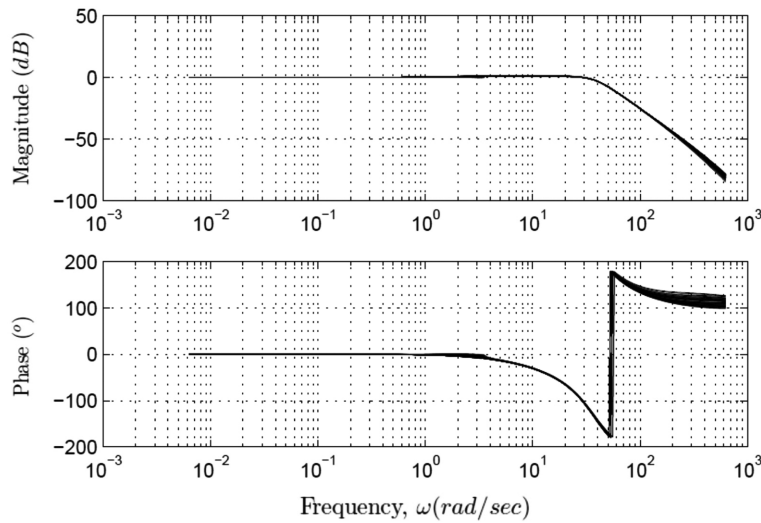


Fig. 9 Frozen parameter bode plots of LPV-GS controller: Transfer function from reference to output

## 5. Simulation results

The key difference between the robust  $\mathcal{H}_\infty$  controller and the LPV-GS controller is that the  $\mathcal{H}_\infty$  controller will not be able to adapt to the change in the system properties. Although the actual system is parameter-varying, robust- $\mathcal{H}_\infty$  controller is designed for a fixed plant (frozen parameters,  $\rho_0$ ) with the nominal parameter values. The parameter variation in the robust- $\mathcal{H}_\infty$  controller design is accounted using the frequency dependent disturbance. So, the performance of the robust- $\mathcal{H}_\infty$  controller depends on how close the actual parameter value,  $\rho$  of the plant to the nominal-parameters,  $\rho_0$ . The closed-loop system with the  $\mathcal{H}_\infty$  controller will be stable only for small parameter variations around the nominal plant parameters,  $\rho_0$ . Whereas the LPV-GS controller is consistently effective for all the parameter variations by taking into account the change in system properties and accommodating into the controller in real time.

To emphasize more on this point, the performance of both the controllers for the ramp SAIVS switching and three pulses of square wave tracking input is calculated. The performance of both the controllers is verified at different input amplitudes but for the sake of conciseness and to be consistent with the experimental results presented in Figs. 4 and 5(a) tracking command of 0.25 inches is presented in this article. The tracking performance of both the controllers is shown in Fig. 10. The nominal values of the parameters used to design the  $\mathcal{H}_\infty$  controller are  $\rho_1 = 0.292$  and  $\rho_2 = 1$ . For the first three jumps in the input (till 400 seconds) the robust- $\mathcal{H}_\infty$  controller and the LPV-GS controller have very similar response characteristics (shown in Fig. 10) but for the subsequent cycles performance of the  $\mathcal{H}_\infty$  controller keeps deteriorating unlike the LVS-GS response which is consistent. This is more evident from the tracking error plot shown in Fig. 11(top). The control force exerted by the actuator is shown in Fig. 11(bottom). It should be noted that the actual force rate calculated from the LPV-GS controller is  $\dot{F}_{ctr}$  from which the control force  $F_{ctr}$  is obtained. Since the  $\mathcal{H}_\infty$  controller is designed for the parameters at  $t=0$  ( $\rho_1 = 0.292$  as shown in Fig. 12), as the system parameters drift away from the nominal plant the performance of the closed-loop system with the  $\mathcal{H}_\infty$  controller deteriorates. For further variation in the linear stiffness of the SAIVS

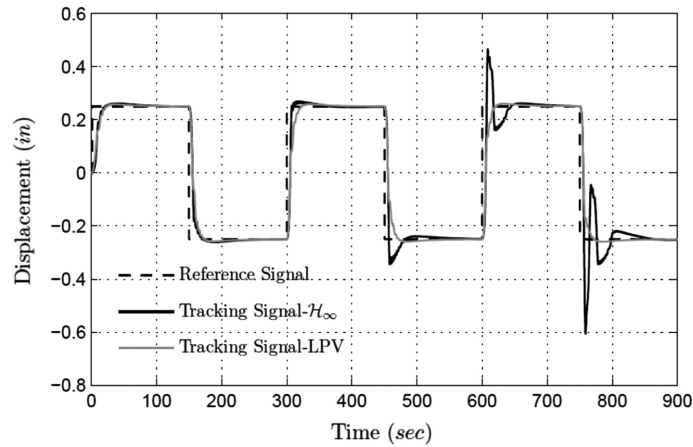


Fig. 10 Tracking response of closed loop SAIVS system to step input using LPVGS controller and  $\mathcal{H}_\infty$ -controller in presence of ramp SAIVS switching

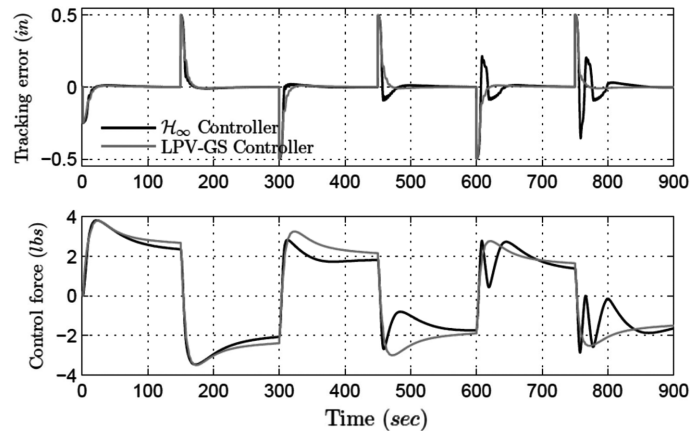


Fig. 11 Comparison of (a) Tracking error of closed loop SAIVS system and (b) control effort exerted by the actuator, using LPV-GS controller and  $\mathcal{H}_\infty$ -controller in presence of ramp SAIVS switching

device, beyond 900 sec, the closed-loop system with the  $\mathcal{H}_\infty$  controller becomes unstable for subsequent cycles.

Linear stiffness of the SAIVS device is decreased from 11.4 lb/in to 4.7 lb/in in 900 seconds using the servo-motor. The change in SAIVS angle,  $\theta$ , is shown in Fig. 12 (top, left) and Fig. 13 (top, left) for systems with  $\mathcal{H}_\infty$  controller and LPV-GS controller respectively. The parameter- $\rho_1$ , calculated using  $\theta$ , is shown in Fig. 12 (top, right) and 13 (top, right). The frictional force measured is shown in Figs. 12 (bottom, left) and Fig. 13 (bottom, left) for systems with the  $\mathcal{H}_\infty$  controller and the LPV-GS controller respectively. The parameter- $\rho_2$  calculated is shown in Figs. 12 (bottom, right) and 13 (bottom, right). For the same desired tracking reference signal and  $\rho_1$ , the frictional force,  $F_d$  (consequently,  $\rho_2$ ) is quite different for the closed-loop system with the  $\mathcal{H}_\infty$  controller and the LPV-GS controller. This is due to the difference in the working principle of the controllers. Since the LPV-GS controller is scheduled based on the parameter  $\rho_2$ , the control input is dependent on the time-history data of  $\rho_2$  and vice-versa. Whereas in the case of  $\mathcal{H}_\infty$  controller control input is only

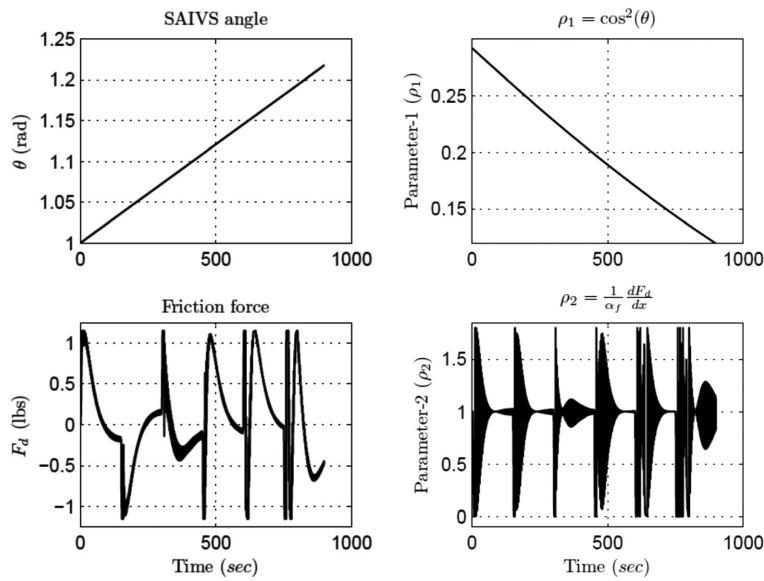


Fig. 12 Parameter variation in closed-loop tracking using  $\mathcal{H}_\infty$ -controller in presence of ramp SAIVS switching. (Top, left): SAIVS angle,  $\theta$ ; (Top, right):  $\rho_1$ ; (Bottom, left): Friction force,  $F_d$ ; (Bottom, right):  $\rho_2$

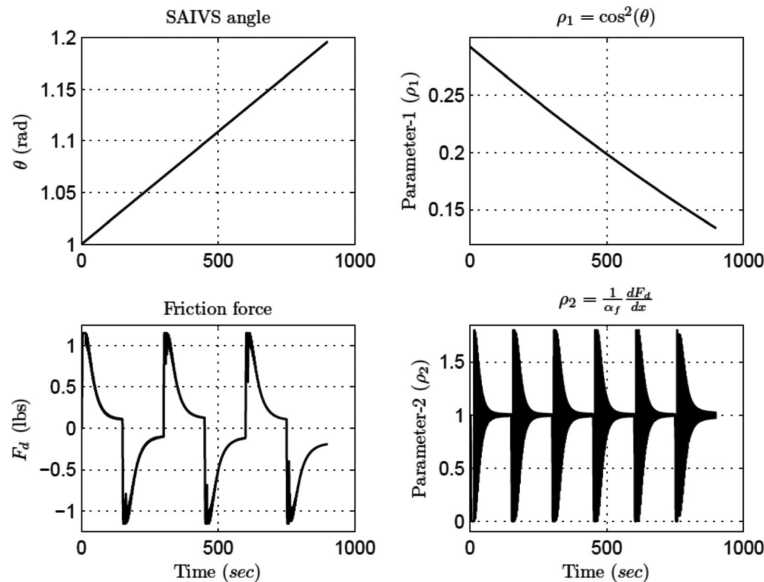


Fig. 13 Parameter variation in closed-loop tracking using LPV-GS controller in presence of ramp SAIVS switching. (Top, left): SAIVS angle,  $\theta$ ; (Top, right):  $\rho_1$ ; (Bottom, left): Friction force,  $F_d$ ; (Bottom, right):  $\rho_2$

influenced by the tracking error.

Hysteresis loops of the closed loop systems are shown in Fig. 14. From Fig. 14 it can be clearly seen that the LPV-GS controller is very effective in controlling the systems with variable hysteresis. Since the linear stiffness of the system is dropping the hysteresis loops in Fig. 14 are tilting in the

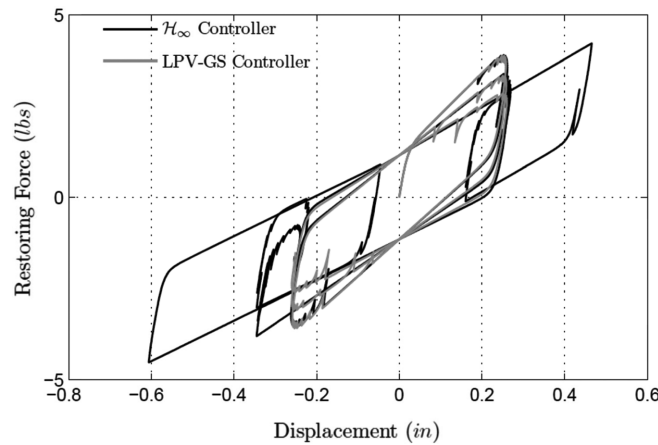


Fig. 14 Comparison of hysteresis loops of step input tracking response in LPV-GS controller and  $\mathcal{H}_\infty$ -controller in presence of ramp SAIVS switching

clockwise direction. Hysteresis loops of the closed-loop system with  $\mathcal{H}_\infty$  controller are wider because of the high overshoot. The key observations that can be made from the Fig. 10 through Fig. 14 are listed below

- (a) LPV-GS controller has smaller settling time and overshoot compared to the  $\mathcal{H}_\infty$  controller.
- (b) Performance of the closed-loop system with the  $\mathcal{H}_\infty$  controller is sensitive to system parameters, unlike the LPV GS controller.
- (c) LPV-GS controller is capable of handling the change in the system parameters by updating the controller.
- (d)  $\mathcal{H}_\infty$  controller becomes unstable for large variations in linear stiffness of the SAIVS device.

## 6. Conclusions

In this paper, hysteretic system with variable stiffness hysteresis is represented as a quasi linear parameter varying system. A gain scheduled controller is designed for the quasi-LPV system using the LMI approach. Designed controller is scheduled based on two parameters: linear time-varying stiffness (slow varying parameter) and the stiffness of friction hysteresis (fast varying parameter). Gain-scheduled controller is constructed from the parameter dependent Lyapunov matrices, which are obtained as the optimal solution of the linear matrix inequalities that ensures the feasibility solution for the closed loop system performance.

To show the effectiveness of the proposed controller numerical studies are carried out comparing the proposed controller with the fixed robust  $\mathcal{H}_\infty$  controller. The tracking performance of the system using both the controllers is verified for different switching cases and for different amplitudes of tracking displacements. Superior performance of the LPV-GS over the robust  $\mathcal{H}_\infty$  controller in different displacement ranges is clearly evident from the reported results. The robust  $\mathcal{H}_\infty$  controller is effective only when the system parameters are in the vicinity of the nominal plant parameters for which the controller is designed. The LPV-GS controller is capable of adapting to the parameter changes and is effective over the entire range of the parameter variations. For large parameter

variations, the robust  $\mathcal{H}_\infty$  controller becomes unstable where as the LPV-GS will ensure stability and guarantee the desired closed-loop performance.

## Acknowledgements

This project is funded by the National Science Foundation under grant NSF-CMMI-0601672 which is gratefully acknowledged.

## References

- Apkarian, P. and Adams, R.J. (1998), "Advanced gain-scheduling techniques for uncertain systems", *IEEE T. Autom.*, **6**(1), 21-32.
- Apkarian, P. and Gahinet, P. (1995), "A convex characterization of gain-scheduled  $\mathcal{H}_\infty$  controllers", *IEEE T. Autom.*, **40**(5), 853-864.
- Apkarian, P., Nemirovski, A., Laub, A. and Chilali, M. (1995), LMI Control Toolbox User's Guide, The MathWorks Inc.: Natick.
- Bai, Y. (2006), *Advanced Controls of Large Scale Structural Systems Using Linear Matrix Inequality Methods*, Ph.D. Thesis, University of Houston, Houston.
- Becker, G.S. (1993), *Quadratic Stability and Performance of Linear Parameter Dependent Systems*, Ph.D. Thesis, Univ. of California, Berkley.
- Bouc, R. (1967), "Forced vibration of mechanical systems with hysteresis", *Proceedings of the 4th Conf. on Nonlin., Oscill.*
- Doyle, J.C., Glover, K., Khargonekar, P.P. and Francis, B.A. (1989), "State-space solutions to standard  $H_2$  and  $H$  control problems", *IEEE T. Autom.*, **34**, 831-847.
- Ganley, T., Hung, D.L.S., Zhu, G and Tan, X. (2011), "Modeling and inverse compensation of temperaturedependent ionic polymer-metal composite sensor dynamics", *IEEE/ASME T. Mechatronics*, **16**(1), 80-89.
- Iyer, R. and Tan, X. (2009), "Control of hysteretic systems through inverse compensation: Inversion algorithms, adaptation, and embedded implementation", *IEEE Contr. Syst. Mag.*, **29**(1), 83-99.
- Krejci, P. and Kuhnen, K. (2001), "Inverse control of systems with hysteresis and creep", *IEEE Proc. Contr. Theory Appl.*, **148**(3), 185-192.
- Liu, S.C. (2008) "Sensors, smart structures technology and steel structures", *Smart Struct. Syst.*, **4**(5), 525-531.
- Mehendale, C.S. (2005), *Advanced Gain-scheduling for Nonlinear Control Design Using Linear Parameter Varying Systems Theory*, Ph.D. Thesis, Univ. of Houston, Houston
- Mehendale, C.S., Fialho, I.J. and Grigoriadis, K.M. (2003), "Adaptive active microgravity isolation using LPV gain-scheduling methods", *Proceedings of the American Control Conference*, Denver, USA.
- Mehendale, C.S. and Grigoriadis, K.M. (2004), "Hysteresis compensation using LPV gain-scheduling", *Am. Control Conf.*, **2**, 1380-1385.
- Mate, D. (1998), *Experimental and analytical study of semiactive variable stiffness control system*, MS Thesis, University of Missouri, Columbia.
- Nagarajaiah, S. and Mate, D. (1998), "Semi-active control of continuously variable stiffness system", *Proceedings of the 2<sup>nd</sup> World Conference on Structural Control*, Tokyo, Japan.
- Nagarajaiah, S. and Sahasrabudhe, S. (2006), "Seismic response control of smart sliding isolated buildings using variable stiffness systems: An experimental and numerical study", *Earthq. Eng. Struct. D.*, **35**(2), 177-197.
- Nagarajaiah, S. and Varadarajan, N. (2005), "Semi-active control of wind excited building with variable stiffness TMD using short time Fourier transform", *Eng. Struct.*, **27**, 431-441.
- Oloomi, H. and Shafai, B. (2003), "Weight selection in mixed sensitivity robust control for improving the sinusoidal tracking performance", *Proceedings of the 42nd IEEE Conference on Decision and Control*.
- Pasala, D.T.R., Nagarajaiah, S. and Grigoriadis, K.M. (2008), "Response control of SAIVS system using LPV gain-scheduling controller", *Proceedings of the Earth and Space Conference*, Long Beach California, USA.

- Pasala, D.T.R., Nagarajaiah, S. and Grigoriadis, K.M. (2009), "Gain scheduled control of hysteretic systems", *Proceedings of the SPIE, Smart Structure/NDE*, San Diego, USA.
- Rugh, W.J. and Shamma, J.S. (2000), "Research on gain scheduling", *Automatica*, **36**(10), 1401-1425.
- Salapaka, S., Sebastian, A., Cleveland, J.P. and Salapaka, M.V. (2002), "High bandwidth nano-positioner: A robust control approach", *Rev. Sci. Instrum.*, **73**(9), 3232-3241.
- Skelton, R.E., Iwasaki, T. and Grigoriadis, K. (1998), *A Unified Algebraic Approach to Linear Control Design*, Taylor & Francis, Great Britain.
- Sivaselvan, M.V. and Reinhorn, A.M. (2000), "Hysteretic Models for Deteriorating Inelastic Structures", *J. Eng. Mech. - ASCE*, **126**(6), 633-40.
- Skogestad, S. and Postlethwaite, I. (1996), *Multivariable Feedback Control: Analysis and Design*, John Wiley & Sons, New York.
- Smith, R.C. (2001), "Inverse compensation for hysteresis in magnetostrictive transducers", *Math. Comput. Model.*, **33**(1-3), 285-298.
- Song, G., Zhao, J., Zhou, X. and Garcia, J. (2005), "Tracking control of a piezoceramic actuator with hysteresis compensation using inverse Preisach model", *IEEE T. Mechatronics*, **10**(2), 198-209.
- Song, G., Ma, N. and Lee, H.J. (2007), "Position estimation and control of SMA actuators based on electrical resistance measurement", *Smart Struct. Syst.*, **3**(2), 189-200.
- Spencer, B.F. and Nagarajaiah, S. (2003), "State of the art of structural control", *J. Struct. Eng. - ASCE*, **129**(7), 845-856.
- Tan, X. and Baras, J.S. (2003), *Adaptive Identification and Control of Hysteresis in Smart Materials*, Tech. Rep. CDCSS TR 2003-3 (ISR TR 2003-40): Univ. of Maryland.
- Taware, A. and Tao, G. (2003), *Control of Sandwich Nonlinear Systems*, Springer-verlag, Heidelberg.
- Wen, Y.K. (1976), "Method for random vibration of hysteretic systems", *J. Eng. Mech. - ASCE*, **102**(2), 249-263.
- Wu, F., Yang, X.H., Packard, A. and Becker, G. (1997), "Induced L<sub>2</sub>-norm control for LPV systems with bounded parameter variation rates", *Int. J. Nonlinear Robust control*.
- Wu, F. (1995), *Control of Linear Parameter Varying Systems*, Ph.D. Thesis Univ. of California, Berkley.
- Wu, F., Yang, X.H., Packard, A. and Becker, G. (1995), "Induced L<sub>2</sub>-norm control for LPV system with bounded parameter variation rates", *Proceedings of the American Control Conference*.
- Zhang, F., Grigoriadis, K.M. and Fialho, I.J. (2009), "Linear parameter-varying control for active vibration isolation systems with stiffness hysteresis", *J. Vib. Control*, **15**, 527-547.
- Zheng, Q. and Wu, F. (2009), "Stabilization of polynomial nonlinear systems using rational Lyapunov functions", *Int. J. Control*, **82**(9), 1605-1615.
- Zapaterio, M., Luo, N., Taylor, E. and Dyke, S.J. (2010), "Modeling and identification of a class of MR fluid foam dampers", *Smart Struct. Syst.*, **6**(2), 101-113.